# Effectiveness of several turbulence models in natural convection

P.C. Walsh and W.H. Leong
*Department of Mechanical, Aerospace and Industrial Engineering, Ryerson University, Toronto, Ontario, Canada*

Received May 2002
Revised August 2003
Accepted September 2003

***Keywords*** *Convection, Heat transfer, Turbulence, Modelling*

***Abstract*** *Heat transfer due to natural convection inside a closed cavity must be modeled to include the effects of turbulence if the Rayleigh number is sufficiently large. This study assesses the performance of several commonly used numerical turbulence models such as k-ε, Renormalized Group k-ε and Reynolds stress model, in predicting heat transfer due to natural convection inside an air-filled cubic cavity. The cavity is maintained at 307 K on one side and 300 K on the opposite side with a linear temperature variation between these values on the remaining walls. Two cases are considered, one in which the heated side is vertical, and the other in which it is inclined at 45° from the horizontal. Rayleigh numbers of $10^7$, $10^8$, $10^9$ and $10^{10}$ are considered. Results of the three turbulence models are compared to experimentally determined values or values from correlations. It was found that the standard k-ε model was the most effective model in terms of accuracy and computational economy.*

## Nomenclature

$C_p$ = constant pressure specific heat of air
ER = expansion rate of the computational grid
$g$ = acceleration due to gravity
$h$ = convection coefficient
$g_i$ = component of gravitational vector
$G_i$ = turbulence production term, $k$-$\varepsilon$ models
$G_{ij}$ = turbulence production term, Reynolds stress model
$k$ = thermal conductivity of air
$L$ = side length of cubical cavity
Nu = average wall Nusselt number, $= q''L/k\Delta T$
$P$ = air pressure
$Pr_t$ = turbulent Prandtl number
$q''$ = average wall heat flux
$R$ = gas constant of air
Ra = Rayleigh number, $= g\beta\rho\Delta T \quad L^3/\mu\alpha$
$T$ = temperature in kelvin
$u_\tau$ = friction velocity
$x$ = arbitrary spatial coordinate
$y$ = normal distance from the wall
$Y^+$ = off-wall Reynolds number, $= \rho u_\tau \; y/\mu$

### *Greek symbols*

$\alpha$ = thermal diffusivity of air, $= k/\rho C_p$
$\beta$ = thermal expansion coefficient of air $= -(\partial\rho/\partial T)_p/\rho$
$\Delta T$ = temperature difference between hot and cold faces of cavity
$\Delta x$ = local numerical grid spacing
$\rho$ = air density
$\mu$ = absolute viscosity of air
$\mu_t$ = turbulent eddy viscosity
$\varphi$ = tilt angle of hot cavity face from the horizontal

### *Subscripts*

c, h = pertaining to the cold and hot walls of the cavity respectively
cor = denotes value determined from correlation
exp = denotes experimentally determined value
$i, j$ = indexing integers
$m$ = mean

International Journal of Numerical Methods for Heat & Fluid Flow
Vol. 14 No. 5, 2004
pp. 633-648

0961-5539
DOI 10.1108/09615530410539955

## Introduction

In numerous industrial settings, heat transfer within enclosed spaces will be influenced by natural convection. If the Rayleigh number of the convective process is sufficiently large, heat transfer will be augmented by turbulent fluid motion. An engineer's first instinct in determining the magnitude of such processes will be to use numerical modeling algorithms with a standard turbulence model such as $k$-$\varepsilon$ (Launder and Spalding, 1972, 1974), Renormalized Group $k$-$\varepsilon$ (Choudhury, 1993), or Reynolds stress model (RSM) (Launder *et al.*, 1975). Although this approach is not erroneous, it does make the dubious assumption that each one of these models is appropriate for the given problem with any variation in respective solutions being attributable to the sophistication of the model's derivation. However, there is no assurance that even a mathematically rigorous model, such as the five-equation will provide any greater accuracy than the two-equation $k$-$\varepsilon$ in a natural convection problem. The only means available to determine the appropriateness of one model over the other is through comparison to a definitive benchmark problem that provides reliable data.

Although many options are available for a simple benchmark test case, one with a physically realizable solution is not readily determined. Consider a simple two-dimensional air-filled square cavity with two adiabatic walls and two isothermal walls of differing temperatures. At first glance it would appear to be a routine matter to construct a model in a laboratory environment. However, as Le Quere (1991) observed, this problem by its very nature was "without physical meaning" for two reasons. Primarily, the adiabatic walls that separate the isothermal boundaries cannot be precisely achieved in an air-filled cavity (El Sherbiny *et al.*, 1982). But also, the assumption of a purely two-dimensional flow field is questionable since three-dimensional perturbations can arise in similar confined spaces (Penot *et al.*, 1990). These difficulties are reflected in the work of a number of researchers (Viskanta *et al.*, 1986; Yguel and Vullierma, 1986; Le Peutrec and Lauriat, 1990) who show discrepancy between analytical and experimental values as a result of non-physical wall assumptions.

The difficulty in the classical cavity problem stems from the corners where an ideally isothermal boundary is in contact with an adiabatic wall. This situation is easily modeled numerically but impossible to implement experimentally with any accuracy. One alternative would be to alter the benchmark problem to accommodate this physical constraint. However, such a modification would be subjective in nature diminishing its usefulness as a benchmark problem. Another alternative would be to replace the adiabatic wall condition with one that is more realizable but as objective as the adiabatic wall. A linear temperature gradient between hot and cold surfaces along the remaining walls is still general in nature but more importantly, it has a greater chance of being accurately recreated in the laboratory. Recent work by

Leong *et al.* (1998, 1999) has shown that a cubic cavity, as shown in Figure 1, with linear temperature gradients in four non-isothermal walls, can be designed carefully to produce an average Nusselt number on the cold wall to an accuracy of about 1.2 percent.

The objective of this study is to use the experimental results of Leong *et al.* to assess the performance of the $k$-$\varepsilon$, RNG $k$-$\varepsilon$, and RSM turbulence models for natural convection problems inside a closed cubic cavity. It is hoped that this study will contribute to a body of knowledge that will guide analysts in accurately modeling enclosed natural convection and provide a basis for future algorithm refinement.

## Experimental approach

The experiments of Leong *et al.* (1998) were conducted on an apparatus consistent with the configuration shown in Figure 1. The temperature of the hot wall was fixed at $T_h = 307$ K, while the cold wall was $T_c = 300$ K. The length of a side of the cube was $L = 0.1272$ m. The Rayleigh number is traditionally defined as

$$\mathrm{Ra} \equiv \frac{g\rho\beta\,\Delta T\,L^3}{\mu\alpha}. \tag{1}$$

Since air at low pressures can be treated as an ideal gas, the Rayleigh number can be written as,

$$\mathrm{Ra} = \frac{gC_p\,\Delta T P^2 L^3}{\mu k R^2 T^3}. \tag{2}$$

Equation (2) indicates that the Rayleigh number can be varied extensively by changing the temperature difference $\Delta T$, air pressure $P$ and cavity size $L$. In the experiments, the Rayleigh number was varied by variation of the air

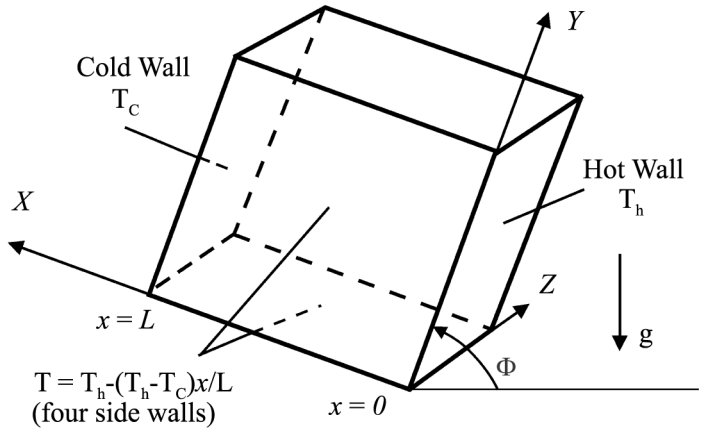


**Figure 1.**
The cubic cavity showing orientation of thermal boundary conditions

pressure inside the cavity, and the air properties were evaluated based on the mean temperature (i.e. $T_m=(T_h+T_c)/2$) and the specific pressure of a desired Ra.

The average Nusselt number on the cold wall is determined by:

$$\mathrm{Nu} \equiv \frac{hL}{k} = \frac{q''L}{k\Delta T}. \tag{3}$$

The average wall heat flux $q''$ was evaluated using an energy balance method (Hollands, 1988) which utilizes a heat flux meter sandwiched between an electrically heated copper plate and an isothermal main copper plate. A heat flux meter is a highly sensitive device which measures temperature differences (and hence heat flux through it) in terms of electrical potential. This method is not intrusive and, hence, it does not disturb or distort the flow in the cavity. Also, unlike any optical method, it does not require any transparent window. Therefore, the linear temperature gradients in the four non-isothermal walls can be achieved using highly conductive copper plates. Although, the radiative heat transfer was found to be very small due to small temperature differences and low emissivity of polished copper surfaces in the cavity, its effects were taken into consideration and corrected when determining the actual convective heat transfer. More details on the experimental methods and their measurement errors can be found in the work of Leong (1996) or Leong *et al.* (1998).

Values of wall average Nusselt number are provided for a variety of inclination angles $\varphi$ and Rayleigh numbers. Since the fundamental behavior of the convection flow will change as the cube is rotated from the horizontal, three cases of inclination angle are considered. At an inclination of $\varphi = 90°$, both isothermal surfaces are oriented vertically, and stable convective boundary layers are formed. At $\varphi = 0°$, the hot surface is at the bottom of the cube with the cold side at the top. In this case, plumes of buoyant fluid will rise from the hot surface towards the cold in an unsteady chaotic manner. These two extreme test cases are selected along with an intermediate case of $\varphi = 45°$.

Rayleigh numbers must be chosen such that the induced convective flow will become turbulent. Markatos and Pericleous (1984) developed a similar square cavity problem with two differentially-heated vertical walls and two adiabatic horizontal walls for $10^3 \leq \mathrm{Ra} \leq 10^{16}$. Based on their findings, they concluded that the effects of turbulence on heat transfer is not significant until $\mathrm{Ra} > 10^6$. Therefore, this investigation begins modeling and comparisons to experiment at a Ra of $10^7$. Leong *et al.* (1998, 1999) were meticulous in designing their experiments and presented a detailed error analysis on their experiments, giving an overall uncertainty of about 1.2 percent on measured Nu values. Experimental values of average Nusselt number for various inclinations and Rayleigh numbers are given in Table I.

Markatos and Pericleous (1984) were able to derive three Nu-Ra correlations from their numerical results for a laminar range ($10^3 \leq \mathrm{Ra} \leq 10^6$) and two

turbulent ranges ($10^6 < \mathrm{Ra} \leq 10^{12}$ and $10^{12} < \mathrm{Ra} \leq 10^{16}$). They also found that their numerical results were in good agreement with an experimental turbulence correlation up to Ra of $10^{12}$, even though the correlation was derived for $2.8 \times 10^4 \leq \mathrm{Ra} \leq 1.55 \times 10^7$. Owing to the findings of Markatos and Pericleous and lack of experimental Nu at higher Ra, it is assumed that the correlations of Leong *et al.* (1999) may be extended up to Ra of $10^{10}$ for comparison with the present predictions. The following are the experimental Nu-Ra correlations from Leong *et al.* (1999):

$$\varphi = 0^\circ: \quad \mathrm{Nu} = 0.1194\,\mathrm{Ra}^{0.3021} \quad 10^5 \leq \mathrm{Ra} \leq 10^8 \tag{4}$$

$$\varphi = 45^\circ: \quad \mathrm{Nu} = 0.1492\,\mathrm{Ra}^{0.2955} \quad 10^6 \leq \mathrm{Ra} \leq 10^8 \tag{5}$$

$$\varphi = 90^\circ: \quad \mathrm{Nu} = 0.08461\,\mathrm{Ra}^{0.3125} \quad 10^4 \leq \mathrm{Ra} \leq 10^8 \tag{6}$$

## Numerical algorithm

The analysis is conducted utilizing the commercial computational fluid dynamics (CFD) code "Fluent" (1996). A number of turbulence models are available within Fluent including $k$-$\varepsilon$, RNG $k$-$\varepsilon$, and the RSM. Fluent is a finite volume solver with a number of near-wall treatments including standard wall functions, non-equilibrium wall functions, and a two-layer zonal model. Given the expected variations in character of the flow field between inclinations of 0 and 90°, a two-layer approach is deemed to be the most appropriate. In this approach, boundary layers are partitioned into two separate zones: a viscous sublayer which remains entirely laminar near the walls, and a fully turbulent region away from the walls. Flow field parameters within the viscous sublayer are determined through a model proposed by Wolfstein (1969), while the turbulent region is treated with the selected turbulence model. Although the $\varphi = 90^\circ$ case was expected to produce readily defined boundary layers appropriate for wall functions, the $\varphi = 0^\circ$ case, with its unsteady convection, was not. In this instance, the boundary layer behavior assumptions inherent to wall functions were not justifiable. The two-layer approach being more general was used exclusively throughout this study. In addition, trial modeling of the $\varphi = 90^\circ$ case with various wall treatments indicated that the two-layer approach produced the most rapid convergence rates.

| Ra | $\varphi = 0^\circ$ (percent) | $\varphi = 45^\circ$ (percent) | $\varphi = 90^\circ$ (percent) |
|---|---|---|---|
| $10^6$ | 7.883± 1.2 | 8.837 ± 1.1 | 6.383 ± 1.1 |
| $10^7$ | 15.38± 1.2 | 17.50 ± 1.2 | 12.98 ± 1.2 |
| $10^8$ | 31.22± 1.4 | 34.52 ± 1.2 | 26.79 ± 1.3 |

**Source:** Leong *et al.*, 1999

**Table I.**
Experimental $\mathrm{Nu}_{\mathrm{exp}}$

The effects of turbulence are introduced into the momentum equations through a buoyancy term derived from the Boussinesq approximation. The fluid properties are treated as polynomial functions of temperature at the specific pressure of a desired Ra value. In the turbulence models, a source term is included to account for turbulent kinetic energy production. For the $k$-$\varepsilon$ models the term has the form:

$$G_i = -\frac{g_i}{\rho}\frac{\mu_t}{\mathrm{Pr}_t}\frac{\partial \rho}{\partial x_i}. \tag{7}$$

In the Reynolds stress formulation, a general production tensor is used:

$$G_{ij} = \beta\frac{\mu_t}{\mathrm{Pr}_t}\left(g_i\frac{\partial T}{\partial x_j} + g_j\frac{\partial T}{\partial x_i}\right). \tag{8}$$

## Grid characteristics

Instances commonly arise in numerical analysis where the character of a boundary layer can be estimated with accuracy, allowing for local grid refinement. Node spacing can be made very small in the normal direction at the wall to capture the expected high gradients there. For the present cavity problem, the presence of a buoyancy induced boundary layer cannot be assured. For the $\varphi = 90°$ case, stable boundary layers on all surfaces can be anticipated due to the vertical orientation of the isothermal surfaces. However, for the $\varphi = 0°$ case this will certainly not be the case. It is not known if grid clustering on the walls will have any effect under these circumstances. Furthermore, if boundary layer refinement is imposed, it is not known how the grid expansion rate from the surface will affect the solution. Therefore, as a precursor to the numerical study, an assessment of the effects of grid off-wall spacing and expansion rate was conducted.

The assessment used two-dimensional grids to allow rapid testing over a wide range of grid configurations. The off-wall spacing was measured as the distance from the wall to the first off-wall point normal to the surface. The expansion rate, ER, of a grid is defined as the ratio of distances between adjacent pairs of nodes in a direction normal to the wall:

$$\mathrm{ER} = \frac{\Delta x_{i+1}}{\Delta x_i} \tag{9}$$

It should be noted that an expansion rate of 1 describes a grid with uniform spacing. The values produced on uniform grids are taken as a benchmark solution for this assessment since their solutions are expected to have a higher level of accuracy compared to non-uniform grids due to their lower truncation error.

Tests are computed for a Rayleigh number of $10^8$ on all three inclination angles using the standard $k$-$\varepsilon$. Four off-wall spacings were used:

0.05, 0.0025, 0.00125, and 0.000625 m. Expansion rates were allowed to vary between 1 and 1.9 at most. The average Nusselt number was computed on the cold wall and comparisons were made based on two parameters. First, the absolute percentage difference between a value on a grid with a given ER, and that obtained on a uniform grid with the same off-wall spacing. Second, the absolute percent difference between values on uniform grids with various off-wall spacings and a uniform grid with 0.0003125 m off-wall spacing.

The average Nusselt numbers found for the $\varphi = 90°$ case are presented in Table II. Each row lists the expansion rate, the Nusselt number, and the absolute percentage difference between the given Nusselt number and the value obtained on the uniform mesh with the same off-wall spacing. Clearly, for a given off-wall spacing, the variation in expansion rate has little effect on the solution. The difference in solutions between a uniform grid and a non-uniform grid does not exceed 6.1 percent. With an expansion rate below 1.3 the difference does not exceed 2 percent. However, if values on uniform grids are compared, as in Table III, an interesting result emerges. The difference in

| ER | Nu | Percentage difference |
|---|---|---|
| *Off-wall = 0.005 m* | | |
| 1.48 | 20.27 | 0.82 |
| 1.30 | 20.33 | 0.54 |
| 1.20 | 20.37 | 0.36 |
| 1.05 | 20.43 | 0.08 |
| 1.00 | 20.44 | – |
| *Off-wall = 0.0025 m* | | |
| 1.87 | 27.87 | 2.30 |
| 1.42 | 28.20 | 1.16 |
| 1.25 | 28.34 | 0.66 |
| 1.20 | 28.37 | 0.54 |
| 1.05 | 28.50 | 0.12 |
| 1.00 | 28.53 | – |
| *Off-wall = 0.00125 m* | | |
| 1.90 | 24.97 | 6.06 |
| 1.51 | 25.77 | 3.07 |
| 1.34 | 26.09 | 1.86 |
| 1.21 | 26.29 | 1.10 |
| 1.10 | 26.44 | 0.53 |
| 1.00 | 26.59 | – |
| *Off-wall = 0.000625 m* | | |
| 1.91 | 24.26 | 2.10 |
| 1.48 | 24.53 | 1.00 |
| 1.31 | 24.66 | 0.50 |
| 1.15 | 24.74 | 0.16 |
| 1.05 | 24.76 | 0.05 |
| 1.00 | 24.78 | – |

**Table II.**
Effect of ER for different off-wall spacings and $\varphi = 90°$

| ER | Nu | Percentage difference |
|---|---|---|
| *Off-wall = 0.005 m* | | |
| 1.48 | 20.24 | 2.37 |
| 1.30 | 20.39 | 1.68 |
| 1.20 | 20.49 | 1.16 |
| 1.05 | 20.66 | 0.32 |
| 1.00 | 20.73 | – |
| *Off-wall = 0.0025 m* | | |
| 1.87 | 25.96 | 3.74 |
| 1.42 | 26.28 | 2.54 |
| 1.25 | 26.79 | 0.65 |
| 1.20 | 26.83 | 0.49 |
| 1.05 | 26.95 | 0.04 |
| 1.00 | 26.96 | – |
| *Off-wall = 0.00125 m* | | |
| 1.90 | 23.41 | 1.94 |
| 1.51 | 22.93 | 0.15 |
| 1.34 | 22.46 | 2.19 |
| 1.21 | 22.54 | 1.86 |
| 1.10 | 22.63 | 1.44 |
| 1.00 | 22.96 | – |
| *Off-wall = 0.000625 m* | | |
| 1.91 | 22.45 | 2.56 |
| 1.48 | 21.72 | 0.79 |
| 1.31 | 21.44 | 2.06 |
| 1.15 | 21.46 | 1.95 |
| 1.05 | 21.52 | 1.67 |
| 1.00 | 21.89 | – |

**Table III.**
Effects of ER for different off-wall spacings and $\varphi = 45°$

Nusselt number between a uniform grid with 0.0025 m off-wall spacing and that of a uniform grid with 0.0003125 m spacing is about 21 percent, a large change. Table III also provides values of the highest observed value of $Y^+$ on the cold wall, which should be of order 1 in a two-layer boundary approach. Even with the largest off-wall spacing considered, the two-layer approach is valid.

Similar results for the $\varphi = 45$ and 0° cases are given also in Tables IV and V. For the $\varphi = 0°$ case it should be noted that the value of Nusselt number was averaged over a long period of time to obtain a fixed value. The results shown for these cases are consistent with those presented in the $\varphi = 90°$ case. Again, changes in grid expansion rates have a much smaller influence on Nusselt number than the off-wall spacing. The implication of this for grid generation is that the selection of an off-wall spacing is of greater importance than the expansion rate. Furthermore, if the off-wall spacing is limited to a maximum of 0.00125 m, the expected $Y^+$ values will be of order 1 meaning that the two-layer boundary model will be valid. Three cubic grids were created with

| ER | Nu | Percentage difference |
|---|---|---|
| *Off-wall = 0.005 m* | | |
| 1.48 | 17.86 | 8.40 |
| 1.30 | 18.29 | 6.19 |
| 1.20 | 18.65 | 4.34 |
| 1.05 | 19.22 | 1.40 |
| 1.00 | 19.49 | – |
| *Off-wall = 0.0025 m* | | |
| 1.87 | 17.92 | 2.54 |
| 1.42 | 17.85 | 2.94 |
| 1.25 | 18.30 | 0.50 |
| 1.20 | 18.30 | 0.50 |
| 1.05 | 18.43 | 0.22 |
| 1.00 | 19.39 | – |
| *Off-wall = 0.00125 m* | | |
| 1.90 | 16.32 | 1.98 |
| 1.51 | 16.39 | 1.62 |
| 1.34 | 16.51 | 0.86 |
| 1.21 | 16.51 | 0.86 |
| 1.10 | 16.65 | 0.00 |
| 1.00 | 16.65 | – |
| *Off-wall = 0.000625 m* | | |
| 1.91 | 15.02 | 7.84 |
| 1.48 | 15.82 | 2.97 |
| 1.31 | 15.88 | 2.57 |
| 1.15 | 16.02 | 1.75 |
| 1.05 | 16.05 | 1.52 |
| 1.00 | 16.30 | – |

**Table IV.** Effects of ER for different off-wall spacings and $\varphi = 0°$

| | $\varphi = 90°$ | | | $\varphi = 45°$ | | | $\varphi = 0°$ | | |
|---|---|---|---|---|---|---|---|---|---|
| Off-wall (m) | Nu | Percentage difference | $Y^+$ | Nu | Percentage difference | $Y^+$ | Nu | Percentage difference | $Y^+$ |
| 0.005 | 20.44 | 12.9 | 6.7 | 20.73 | 5.88 | 7.6 | 19.49 | 26.48 | 6.2 |
| 0.0025 | 28.53 | 21.55 | 5.3 | 26.96 | 22.39 | 4.8 | 18.39 | 19.33 | 2.4 |
| 0.00125 | 26.59 | 13.27 | 3.3 | 22.96 | 0.04 | 2.7 | 16.65 | 8.05 | 1.2 |
| 0.000625 | 24.78 | 5.58 | 1.7 | 21.89 | 0.01 | 1.4 | 16.30 | 5.78 | 0.5 |
| 0.0003125 | 23.47 | – | 0.9 | 22.03 | – | 0.8 | 15.41 | – | 0.3 |

**Table V.** Effects of uniform grid sizes for different inclination angles $\varphi$

varying degrees of refinement, allowing an assessment of the sensitivity of each model to grid resolution. The details of each grid are specified in Table VI.

A number of significant findings can be concluded from the results of the grid characteristic study. Primarily, the initial off-wall spacing has a stronger

influence on solution accuracy than does grid expansion rate. Although the off-wall finding may not in general be novel, in the context of the enclosed cubic cavity with the range of thermal boundary conditions considered it is significant. Finally, this analysis provides the guidance for generating the three model grids and the verification for use of the two layer approach for each grid.

## Results and discussion

The case where the inclination is 0° and the hot surface is on the bottom of the cube, is somewhat of a pariah. Convectional instabilities lead to chaotic fluid motion making an unsteady numerical solution difficult to achieve. In spite of time averaging of the cold-wall Nusselt number the numerical values do not compare well with the experiment. In Figure 2, the average Nusselt number is plotted as a function of time for the $30 \times 30 \times 30$ grid with $Ra = 10^8$, $\varphi = 0°$, and the standard $k$-$\varepsilon$ model. Taking a time average of the Nusselt number yields a value of 19.9 compared to 31.22 in the experiment. Further, grid refinement does not alter these poor numerical results appreciably. Similar under-predictions of about 35-40 percent compared to the correlated Nusselt number ($Nu_{cor}$) by equation (4) are also obtained for Ra of $10^9$ with all the three

| Layout | Off-wall (m) | ER | Nodes |
|---|---|---|---|
| $15 \times 15 \times 15$ | 0.00125 | 1.6 | 4,096 |
| $30 \times 30 \times 30$ | 0.000625 | 1.24 | 2,9791 |
| $60 \times 60 \times 60$ | 0.0003125 | 1.11 | 22,6981 |

**Table VI.**
Test grid specifications

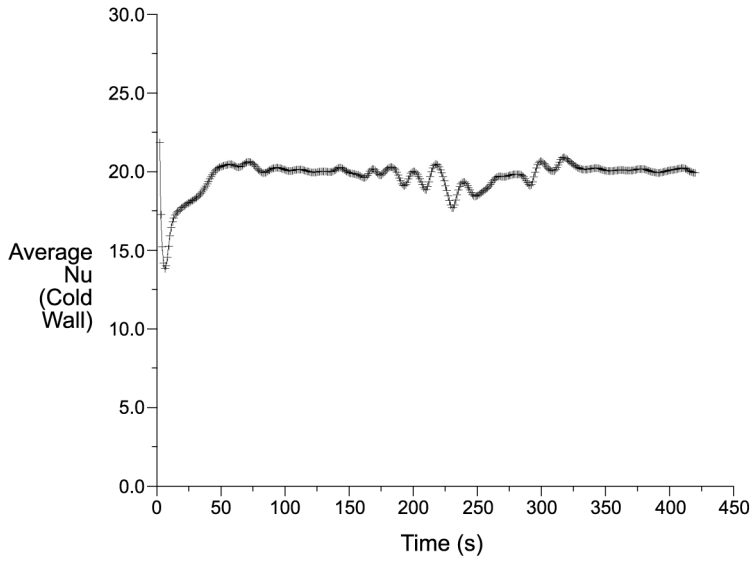


**Figure 2.**
The average Nusselt number on the cold wall for $Ra = 10^8$, $\varphi = 0°$ vs time. Time averaged $Nu = 19.9$, while $Nu_{exp} = 31.22$

grid sizes and three turbulence models. As an additional test, the same case is recomputed with a Rayleigh number of $10^6$ as a case of laminar natural convection flow. The result is shown in Figure 3, producing a time average Nusselt number of 7.44 which compares more favourably to the experimental value of 7.88. This result suggests that turbulent heat transport is not being modeled correctly. Since the laminar case with the same grid produced a far better result, the only conclusion that can be reached is that a degree of modeling difficulty exists in turbulent natural convection associated with the heating-from-below case. The two other turbulence models considered did not alter this conclusion. For this reason, further analysis using the $\varphi = 0°$ case was not presented. Clearly, further work for unsteady turbulence modeling of natural convection flows for this case is needed.

The results of the $\varphi = 90$ and 45° cases compared significantly better to experimental values. Results for $Ra = 10^7$ and $10^8$ are presented in Tables VII-IX for the grid sizes $15 \times 15 \times 15$, $30 \times 30 \times 30$, and $60 \times 60 \times 60$, respectively. Whereas, for $Ra = 10^9$ and $10^{10}$, Tables X-XII tabulate the results for the respective three grid sizes. The performance of each turbulence model is assessed by a comparison of the percent absolute difference between the computed cold-wall Nusselt number and the experimental or correlational value for each grid size, inclination and Rayleigh number. For the case of $Ra = 10^7$ and $\varphi = 90°$, both standard $k$-$\varepsilon$ and RNG $k$-$\varepsilon$ do equally well with errors less than 2 percent. The RSM produces approximately twice the error for this case than the $k$-$\varepsilon$ models. For this low intensity turbulence problem, the $k$-$\varepsilon$ models appear more adept at resolving the vertically driven boundary layers. If the Rayleigh number is increased to $10^8$, the differences between the models

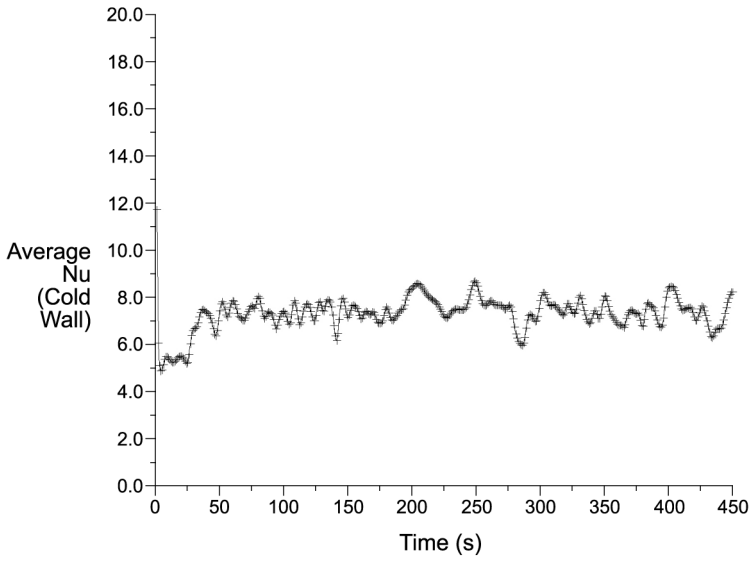


**Figure 3.**
The average Nusselt number on the cold wall for $Ra = 10^6$, $\varphi = 0°$ vs time. Time averaged $Nu = 7.44$, while $Nu_{exp} = 7.88$

disappear and the error values increase to levels approaching 10 percent. As the Ra number is increased further to $10^9$ and $10^{10}$ in the $\varphi = 90°$ case, errors remain relatively close to 10 percent for both $k$-$\varepsilon$ models but are somewhat higher for the RSM. The comparison to experiment also reveals that for the higher Ra numbers, each model tends to under predict the turbulence enhanced heat transfer rate, except for two cases of $k$-$\varepsilon$ model (with $Ra = 10^9$ at $15 \times 15 \times 15$ grid size and $Ra = 10^{10}$ at $30 \times 30 \times 30$ grid size). This apparent

**Table VII.**
Difference with respect to $Nu_{exp}$ and ranking of turbulence models for $15 \times 15 \times 15$ grid

| | $Ra = 10^7$ | | | | | | $Ra = 10^8$ | | | | | |
|---|---|---|---|---|---|---|---|---|---|---|---|---|
| | 45° ($Nu_{exp}$=17.50) | | | 90° ($Nu_{exp}$=12.98) | | | 45° ($Nu_{exp}$=34.52) | | | 90° ($Nu_{exp}$=26.79) | | |
| Model | Nu | Percentage difference | Rank | Nu | Percentage difference | Rank | Nu | Percentage difference | Rank | Nu | Percentage difference | Rank |
| Std. $k$-$\varepsilon$ | 14.29 | 18.3 | 2 | 12.79 | 1.5 | 2 | 26.42 | 23.5 | 2 | 25.39 | 5.2 | 1 |
| RNG $k$-$\varepsilon$ | 14.13 | 19.3 | 3 | 12.83 | 1.2 | 1 | 25.65 | 25.7 | 3 | 24.91 | 7.0 | 2 |
| RSM | 14.33 | 18.1 | 1 | 12.53 | 3.5 | 3 | 26.87 | 22.2 | 1 | 24.87 | 7.2 | 3 |

**Table VIII.**
Difference with respect to $Nu_{exp}$ and ranking of turbulence models for $30 \times 30 \times 30$ grid

| | $Ra = 10^7$ | | | | | | $Ra = 10^8$ | | | | | |
|---|---|---|---|---|---|---|---|---|---|---|---|---|
| | 45° ($Nu_{exp}$=17.50) | | | 90° ($Nu_{exp}$=12.98) | | | 45° ($Nu_{exp}$=34.52) | | | 90° ($Nu_{exp}$=26.79) | | |
| Model | Nu | Percentage difference | Rank | Nu | Percentage difference | Rank | Nu | Percentage difference | Rank | Nu | Percentage difference | Rank |
| Std. $k$-$\varepsilon$ | 16.21 | 7.4 | 2 | 12.88 | 0.77 | 2 | 28.53 | 17.4 | 1 | 24.37 | 9.0 | 1 |
| RNG $k$-$\varepsilon$ | 16.26 | 7.1 | 1 | 12.95 | 0.23 | 1 | 28.01 | 18.9 | 3 | 24.36 | 9.1 | 2 |
| RSM | 15.56 | 11.1 | 3 | 12.45 | 4.1 | 3 | 28.06 | 18.7 | 2 | 24.06 | 10.2 | 3 |

**Table IX.**
Difference with respect to $Nu_{exp}$ and ranking of turbulence models for $60 \times 60 \times 60$ grid

| | $Ra = 10^7$ | | | | | | $Ra = 10^8$ | | | | | |
|---|---|---|---|---|---|---|---|---|---|---|---|---|
| | 45° ($Nu_{exp}$=17.50) | | | 90° ($Nu_{exp}$=12.98) | | | 45° ($Nu_{exp}$=34.52) | | | 90° ($Nu_{exp}$=26.79) | | |
| Model | Nu | Percentage difference | Rank | Nu | Percentage difference | Rank | Nu | Percentage difference | Rank | Nu | Percentage difference | Rank |
| Std. $k$-$\varepsilon$ | 16.40 | 6.3 | 2 | 12.92 | 0.46 | 2 | 28.00 | 18.9 | 1 | 24.29 | 9.3 | 2 |
| RNG $k$-$\varepsilon$ | 16.42 | 6.3 | 1 | 13.00 | 0.15 | 1 | 27.08 | 21.6 | 2 | 24.36 | 9.1 | 1 |
| RSM | 15.58 | 11.0 | 3 | 12.45 | 4.1 | 3 | 25.58 | 25.9 | 3 | 23.98 | 10.5 | 3 |

weakness is even more evident when a level of instability is introduced as in the $\varphi = 45°$ case. Here, the predicted Nusselt numbers are as much as 25 percent or more below the experimental values. It should also be noted that grid refinement had little effect on the final outcome. For the low turbulence intensity cases, $Ra = 10^7$, only a slight improvement was achieved with grid refinement. For the more intense turbulence cases, such as for $Ra \geq 10^8$, no discernable benefit is seen with grid refinement. In some cases, grid refinement leads to poorer results, suggesting that the error seen is due to turbulence modeling and not an under-resolved flow field.

| | $Ra = 10^9$ | | | | | | $Ra = 10^{10}$ | | | | | |
|---|---|---|---|---|---|---|---|---|---|---|---|---|
| | 45° ($Nu_{cor}$ = 68.12) | | | 90° ($Nu_{cor}$ = 54.94) | | | 45° ($Nu_{cor}$ = 134.5) | | | 90° ($Nu_{cor}$ = 112.8) | | |
| Model | Nu | Percentage difference | Rank | Nu | Percentage difference | Rank | Nu | Percentage difference | Rank | Nu | Percentage difference | Rank |
| Std. $k$-$\varepsilon$ | 59.92 | 12.0 | 2 | 59.42 | 8.1 | 2 | 107.6 | 20.0 | 2 | 107.5 | 4.7 | 2 |
| RNG $k$-$\varepsilon$ | 60.60 | 11.0 | 1 | 59.99 | 9.2 | 3 | 108.4 | 19.4 | 1 | 108.6 | 3.7 | 1 |
| RSM | 54.83 | 19.5 | 3 | 54.92 | 0.05 | 1 | 93.6 | 30.4 | 3 | 84.02 | 25.5 | 3 |

**Table X.** Difference with respect to $Nu_{cor}$ and ranking of turbulence models for $15 \times 15 \times 15$ grid

| | $Ra = 10^9$ | | | | | | $Ra = 10^{10}$ | | | | | |
|---|---|---|---|---|---|---|---|---|---|---|---|---|
| | 45° ($Nu_{cor}$ = 68.12) | | | 90° ($Nu_{cor}$ = 54.94) | | | 45° ($Nu_{cor}$ = 134.5) | | | 90° ($Nu_{cor}$ = 112.8) | | |
| Model | Nu | Percentage difference | Rank | Nu | Percentage difference | Rank | Nu | Percentage difference | Rank | Nu | Percentage difference | Rank |
| Std. $k$-$\varepsilon$ | 53.30 | 21.7 | 2 | 49.95 | 9.09 | 2 | 115.8 | 13.9 | 2 | 118.4 | 4.9 | 1 |
| RNG $k$-$\varepsilon$ | 54.20 | 20.4 | 1 | 50.80 | 7.54 | 1 | 120.0 | 10.8 | 1 | 120.8 | 7.1 | 2 |
| RSM | 50.05 | 26.5 | 3 | 48.55 | 11.6 | 3 | 107.2 | 20.3 | 3 | 104.1 | 7.8 | 3 |

**Table XI.** Difference with respect to $Nu_{cor}$ and ranking of turbulence models for $30 \times 30 \times 30$ grid

| | $Ra = 10^9$ | | | | | | $Ra = 10^{10}$ | | | | | |
|---|---|---|---|---|---|---|---|---|---|---|---|---|
| | 45° ($Nu_{cor}$ = 68.12) | | | 90° ($Nu_{cor}$ = 54.94) | | | 45° ($Nu_{cor}$ = 134.5) | | | 90° ($Nu_{cor}$ = 112.8) | | |
| Model | Nu | Percentage difference | Rank | Nu | Percentage difference | Rank | Nu | Percentage difference | Rank | Nu | Percentage difference | Rank |
| Std. $k$-$\varepsilon$ | 50.61 | 25.7 | 2 | 47.30 | 13.9 | 2 | 107.8 | 19.9 | 1 | 103.0 | 8.7 | 2 |
| RNG $k$-$\varepsilon$ | 51.34 | 24.6 | 1 | 47.65 | 13.3 | 1 | 106.9 | 20.5 | 2 | 106.5 | 5.6 | 1 |
| RSM | 48.51 | 28.8 | 3 | 47.01 | 14.4 | 3 | 96.7 | 28.1 | 3 | 93.1 | 17.5 | 3 |

**Table XII.** Difference with respect to $Nu_{cor}$ and ranking of turbulence models for $60 \times 60 \times 60$ grid

An alternative means of assessing the performance of each model is to use a decision matrix based on relative rankings, as indicated in Tables VII-IX for lower turbulence intensity and Tables X-XII for higher turbulence intensity. For instance, the lowest error model for a particular case is assigned a rank of "1", while the poorest receives "3". A sum of the rankings will provide an indication of overall performance. In addition, general performance can also be evaluated by the average of the percentage errors. Tables XIII-XIV tabulate the sums of the rankings and averages of the errors according to turbulence intensities and orientations. Clearly, from the overall performance, the three turbulence models are at least 10 percent better in predicting the $\varphi = 90°$ case with vertical boundary layer than the $\varphi = 45°$ case. The performance of the standard $k$-$\varepsilon$ and RNG $k$-$\varepsilon$ models are almost identical for the lower turbulence intensity cases with 20 and 21 points, respectively, while the RSM is generally poorer with a score of 31. With 1.2 percent and 0.1 percent less error for the $\varphi = 45$ and 90°, respectively, the standard $k$-$\varepsilon$ is preferred over the RNG $k$-$\varepsilon$ model for the lower turbulence intensity cases. However, for the higher turbulence intensity cases, the RNG $k$-$\varepsilon$ performs better than the standard $k$-$\varepsilon$ model with 1.1 percent and 0.5 percent less error for the $\varphi = 45$ and 90°, respectively. Also the RNG $k$-$\varepsilon$ out-performs the standard $k$-$\varepsilon$ model by six points, while it out-performs the RSM by 18 points in the higher turbulence intensity cases. If the computational cost associated with each model is also considered, the standard $k$-$\varepsilon$ is viewed more favorably than the RNG $k$-$\varepsilon$ model, due to the fact that the RNG $k$-$\varepsilon$ with some additional cost above that of the standard $k$-$\varepsilon$ does not improve the results significantly for the higher turbulence intensity cases. The additional cost for computation and storage for the RSR is significantly higher than the $k$-$\varepsilon$ models owing to the larger number of equations solved and variables stored. Generally, the RSM produces results

**Table XIII.**
Overall performance for $Ra = 10^7$ and $10^8$ (lower turbulence intensity cases)

| Model | 45° Sum of rank | 45° Average of errors (percent) | 90° Sum of rank | 90° Average of errors (percent) | Overall Sum of rank | Overall Average of errors (percent) |
|---|---|---|---|---|---|---|
| Std. $k$-$\varepsilon$ | 10 | 15.3 | 10 | 4.4 | 20 | 9.8 |
| RNG $k$-$\varepsilon$ | 13 | 16.5 | 8 | 4.5 | 21 | 10.5 |
| RSM | 13 | 17.8 | 18 | 6.6 | 31 | 12.2 |

**Table XIV.**
Overall performance for $Ra = 10^9$ and $10^{10}$ (higher turbulence intensity cases)

| Model | 45° Sum of rank | 45° Average of errors (percent) | 90° Sum of rank | 90° Average of errors (percent) | Overall Sum of rank | Overall Average of errors (percent) |
|---|---|---|---|---|---|---|
| Std. $k$-$\varepsilon$ | 11 | 18.9 | 11 | 8.2 | 22 | 13.5 |
| RNG $k$-$\varepsilon$ | 7 | 17.8 | 9 | 7.7 | 16 | 12.8 |
| RSM | 18 | 25.6 | 16 | 12.8 | 34 | 19.2 |

with significantly higher errors than the $k$-$\varepsilon$ models, especially for the higher turbulence intensity case.

## Conclusions and recommendations

This study presents a comparison between the predicted values of average Nusselt number and experimental or correlated results for three turbulence models: standard $k$-$\varepsilon$, RNG $k$-$\varepsilon$, and RSM. All comparisons where made for an air-filled cubic cavity over Rayleigh numbers of $10^7$, $10^8$, $10^9$ and $10^{10}$ and two geometrical configurations. The conclusions drawn from this work can be summarized in the following points.

(1) No turbulence model considered could adequately reproduce the experimental results for the unstable case with heating-from-bottom surface ($\varphi = 0°$). A laminar flow calculation for a lower Rayleigh number demonstrated that the significant error was due to the inability of each model to estimate the buoyancy induced turbulence intensity.

(2) Further evidence of modeling difficulty was apparent when grid refinement was considered. For all Rayleigh numbers considered and both hot-wall orientations ($\varphi = 45°$ and 90°) no significant benefit was observed with grid refinement. This suggests that the errors observed were due to turbulence modeling in natural convection and not due to an under-resolved flow field.

(3) For low intensity turbulence with $\mathrm{Ra} = 10^7$ and vertical heated walls, $\varphi = 90°$, the $k$-$\varepsilon$ models were able to predict the cold-wall Nusselt number to within 2 percent of the experimental value, while the RSM did somewhat worse. As the Ra was increased to $10^8$, the differences between the models lessened and the error increased to about 10 percent. However further increase in Ra leads to greater differences between models, and the errors generally remain within about 10 percent for the $k$-$\varepsilon$ models and somewhat worse for the Reynolds stress model. For problems with distinct boundary layers ($\varphi = 90°$), the standard $k$-$\varepsilon$ model performs as well as any model considered, but with the lowest computational cost.

(4) For the partially inclined heated surface cases, $\varphi = 45°$, error was generally higher. As the turbulence intensity increased, the error increased as well reaching an average value of about 18 percent for the $k$-$\varepsilon$ models and about 26 percent for the RSM. In some instances, the RSM had almost twice the error as the $k$-$\varepsilon$ models. Again, the standard $k$-$\varepsilon$ model performs almost as well as the RNG $k$-$\varepsilon$ model for the $\varphi = 45°$ case, but with lower computational cost.

(5) The RSM did not improve on the results of either of the other models in any case. In light of this and its substantially greater computational cost, the RSM is not appropriate for air-filled closed cavity natural convection problems.

## References

Choudhury, D. (1993), "Introduction to the renormalization group method and turbulence modeling", Fluent Inc., Technical Memo 107.

El Sherbiny, S.M., Hollands, K.G. and Raithby, G.D. (1982), "Effect of thermal boundary conditions on natural convection in vertical and inclined air layers", *Journal of Heat Transfer*, Vol. 104, pp. 515-20.

"Fluent 5" (1996), *Fluent User's Manual*, New Hemisphere pub.

Hollands, K.G.T. (1988), "Direct measurement of gaseous natural convective heat fluxes", in Shah, R.K., Ganic, E.N. and Yang, K.T. (Eds), *Experimental Heat Transfer, Fluid Mechanics and Thermodynamics*, Elsevier, New York, pp. 160-8.

Launder, B.E. and Spalding, D.B. (1972), *Lectures in Mathematical Models of Turbulence*, Academic Press, London.

Launder, B.E. and Spalding, D.B. (1974), "The numerical computation of turbulent flows", *Computer Methods in Applied Mechanics and Engineering*, Vol. 3, pp. 269-84.

Launder, B.E., Reece, G.J. and Rodi, W. (1975), "Progress in the development of a Reynolds stress turbulence closure", *Journal of Fluid Mechanics*, Vol. 68 No. 3, pp. 537-66.

Leong, W.H., (1996) "Benchmark experiments on natural convection heat transfer across a cubical cavity PhD thesis", Department of Mechanical Engineering, University of Waterloo, Waterloo, Ontario.

Leong, W.H., Hollands, K.G. and Brunger, A.P. (1998), "On a physically-realizable benchmark problem in natural convection", *International Journal of Heat and Mass Transfer*, Vol. 41, pp. 3817-28.

Leong, W.H., Hollands, K.G. and Brunger, A.P. (1999), "Experimental Nusselt numbers for a cubical-cavity benchmark problem in natural convection", *International Journal of Heat and Mass Transfer*, Vol. 42, pp. 1979-89.

Le Peutrec, Y. and Lauriat, G. (1990), "Effects of heat transfer at the side walls on natural convection cavities", *Journal of Heat Transfer*, Vol. 112, pp. 370-8.

Le Quere, P. (1991), "Accurate solutions to the square thermally driven cavity at high Reynolds number", *Computers and Fluids*, Vol. 20 No. 1, pp. 29-41.

Markatos, N.C. and Pericleous, K.A. (1984), "Laminar and turbulent natural convection in an enclosed cavity", *International Journal of Heat and Mass Transfer*, Vol. 27, pp. 755-72.

Penot, F., N'Dame, A. and Le Quere, P. (1990), "Investigation of the route to turbulence in a vertical differentially heated cavity", *Proceedings of the 9th International Heat Transfer Conference*, Jerusalem, Vol. 2, pp. 417-22.

Viskanta, R., Kim, D.M. and Gau, C. (1986), "Three-dimensional natural convection heat transfer of a liquid metal in a cavity", *International Journal of Heat and Mass Transfer*, Vol. 29 No. 3, pp. 475-85.

Wolfstein, M. (1969), "The velocity and temperature distribution of one-dimensional flow with turbulence augmentation and pressure gradient", *Journal of Heat and Mass Transfer*, Vol. 12, pp. 301-18.

Yguel, F. and Vullierma, J.J. (1986), "Experimental study of high Rayleigh number three-dimensional natural convection in air", *Significant Questions in Buoyancy Affected Enclosure or Cavity Flows*, HTD-60, American Society of Mechanical Engineers, pp. 37-44.